Electrical and Electronic Engineering. 2011; 1(1): 5-11
DOI: 10.5923/j.eee.20110101.02

Hemispherical Dielectric Resonator Antenna Mounted On or Embedded in Spherical Ground Plane with A Superstrate

S. H. Zainud-Deen[1], Noha A. El-Shalaby[2,*], K. H. Awadalla[1]

[1]Faculty of Electronic Engineering, Menoufia University, Menoufia, 32952, Egypt
[2]Faculty of Engineering, Kafrelsheikh University, Kafrelsheikh, 3317, Egypt

Abstract Characteristics of hemispherical dielectric resonator antenna (DRA) mounted on or embedded in spherical ground plane are discussed in this paper. Curvature effects on radiation characteristics of hemispherical DRA are evaluated using the finite element method and the finite integration technique. The co-polarization and the cross-polarization characteristics are analyzed. The structure of a superstrate-loaded hemispherical DRA is treated. The superstrate layer is loaded directly on the hemispherical DRA. The results obtained for the reflection coefficient, the input impedance and the radiation pattern in different planes are analyzed as functions of ground sphere radius and superstrate permittivity.

Keywords DRA, FEM, FIT

1. Introduction

Dielectric resonator antennas (DRAs) have been of interest of the last two and half decades due to its attractive features like high radiation efficiency (virtually no metallic loss and surface wave loss), shape flexibility (rectangular, cylindrical, hemispherical, etc.), different available feeding mechanism (coaxial probes, slots, microstrip lines, coplanar waveguides), a wide range of available material (relative dielectric constant from 4 to 100) , easily controlled characteristics (input impedance, bandwidth, radiation pattern), lightweight, and small size.

Extensive effort was devoted to compute the characteristics of DRA on planar ground plane[1-7]. Numerous applications for DRAs, especially in satellite, missiles, aircraft, spacecraft and mobile communications, require them to be mounted on non-planar surfaces. In these applications, the radiation pattern with low sidelobe characteristics should be provided in order to avoid electromagnetic interference. Improved bandwidth, large angle of coverage, and omnidirectional radiation pattern are several advantage of using antennas over non-planar surfaces. Recently, the radiation characteristics of cylindrical DRA placed on or embedded in circular cylindrical ground plane of finite length are investigated[8-9].

In this paper, the radiation characteristics of hemispherical DRA mounted on or embedded in spherical ground plane structure are investigated. The spherical surface provides more freedom of curvature variation in the θ and φ directions than does the cylindrical structure, which has only one degree of freedom in the φ direction. Numerical results are obtained using the finite element method (FEM)[10] and the finite integration technique (FIT)[11]. The results obtained for the reflection coefficient, the input impedance and the radiation pattern in different planes are analyzed as functions of ground sphere radius and superstrate permittivity.

* Corresponding author:
noha1511ahm@yahoo.com (noha el shalaby)
Published online at http://journal.sapub.org/eee

2. Methods of Solution

2.1. Finite Element Method

The finite element method (FEM) is used for finding approximate solution of partial differential equations (PDE) and integral equations. The solution approach is based either on eliminating the differential equation completely (steady state problems), or rendering the PDE into an equivalent ordinary differential equation, which is then solved using standard techniques such as finite differences. In solving partial differential equations, the primary challenge is to create an equation which approximates the equation to be studied, but which is numerically stable, meaning that errors in the input data and intermediate calculations do not accumulate and cause the resulting output to be meaningless. There are many ways of doing this, all with advantages and disadvantages. The finite element method is a good choice for solving partial differential equations over

complex domains or when desired precision varies over the entire domain. More details about FEM can be found in[10-16].

2.2. Finite Integration Technique

The finite integration technique (FIT) is a spatial discretization scheme to solve electromagnetic field problems in time and frequency domain numerically. FIT was proposed in 1977 by Thomas Weiland[17-20] and has been enhanced continually over the years. This method covers the full range of electromagnetic, from static up to high frequency and optic applications. The basic idea of this approach is to apply the Maxwell's equations in integral form to a set of staggered grids. This method stands out due to high flexibility in geometric modelling and boundary handling as well as incorporation of arbitrary material distributions and material properties such as anisotropy, non-linearity and dispersion. Furthermore, the use of a consistent dual orthogonal grid (e.g. Cartesian grid) in conjunction with an explicit time integration scheme (e.g. leap-frog-scheme) leads to extremely high efficient algorithms referred to both computation time and memory requirements which are especially adapted for transient field analysis in RF applications. More details about FIT can be found in[11].

3. Numerical Results

Figure.1 shows the geometry of hemispherical DRA antenna mounted on metallic ground sphere (filled with air). The metallic ground sphere is assumed to be perfect conductor and the thickness is negligible since it is much less than that of the operating wavelength. The hemispherical DRA with dielectric constant εr =8.9 is used. It has radius "a", of 2.54 cm. A coaxial probe with radius of 0.075 cm excites the antenna. The probe is located off the center by df =1.74 cm with a height "h", of 1.52 cm. The hemispherical DRA is designed to operate at 1.77 GHz. The radius of the ground sphere is "rs".

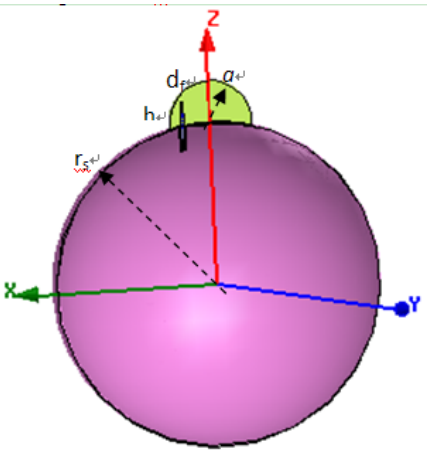

Figure 1. The geometry of hemisphere DRA mounted on spherical ground plane structure.

The simulated reflection coefficient and the input impedance as a function of frequency are illustrated in Figure 2 and Figure 3, respectively. The radius of the sphere, rs =10 cm. The simulated results are calculated by using the FEM and compared with that calculated by FIT method. Good agreement is obtained. The effect of changing the radius of the sphere, rs, on the reflection coefficient, input impedance and resonant frequency are demonstrated in Figs.4-6. It is seen that the resonant frequency increases with increasing the radius of the sphere. The resonant input resistance occurs at higher frequencies for larger sphere radii. The input resistance and reactance levels are also seen to be little decrease with increasing sphere radii.

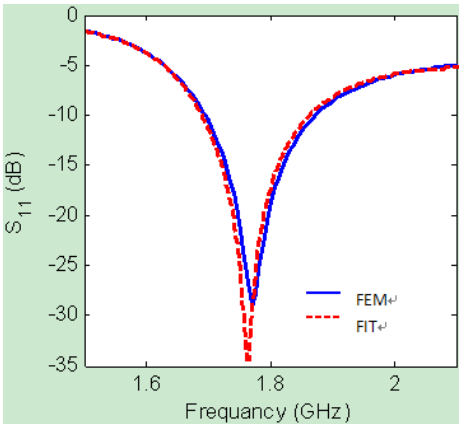

Figure 2. Reflection coefficient versus frequency for rs=10cm.

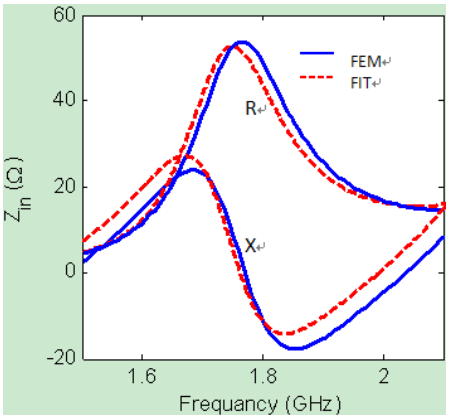

Figure 3. Input impedance versus frequency for r_s=10cm.

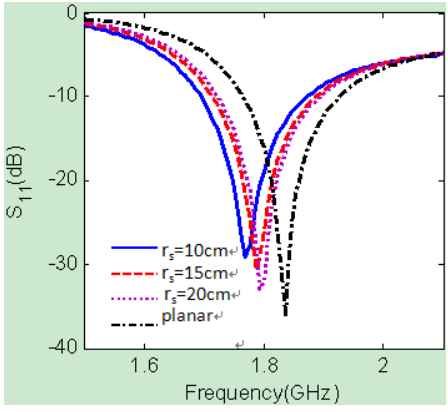

Figure 4. Reflection coefficient versus frequency for different sphere radii, r_s.

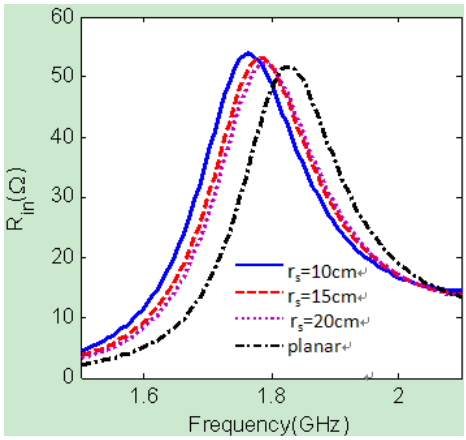

a. input resistance.

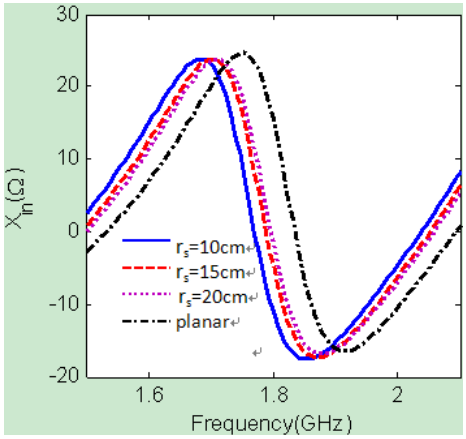

b. input reactance.

Figure 5. Input impedance for different sphere radii, rs.

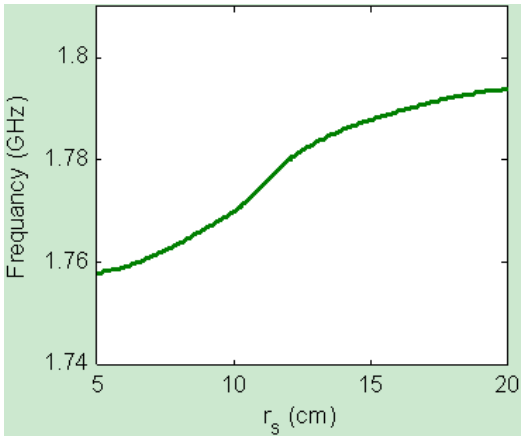

Figure 6. The resonance frequency versus different sphere radii, rs.

The FEM method is used to simulate the radiation patterns in different planes as shown in Figure7. The radius of the sphere rs =10 cm and the operating frequency, f =1.77GHz. The results are compared with that calculated by FIT method. Good agreement is depicted. The copolarized and the cross-polarized field components are shown in Figure8, Ecopol = Eθ cosφ - Eφ sinφ, Expol = Eθ sinφ + Eφ cosφ, the field amplitudes in each case are normalized with respect to the copolarized field at θ = 0. The effects of changing the sphere radii on the polarized field components are illustrated in Figure9. Little variation in the cross-polarization field component with increasing the sphere radii is noticed. The back radiation is seen to increase with decreasing the sphere radius. Figure10 shows the cross-polarization level, Ecopol./Expol., as a function of frequency. It is seen that as the radius of the sphere increases, the cross-polarization level increases. This means that the hemispherical DRA on the spherical ground plane structure has a better linear polarization characteristic than that in planar ground plane.

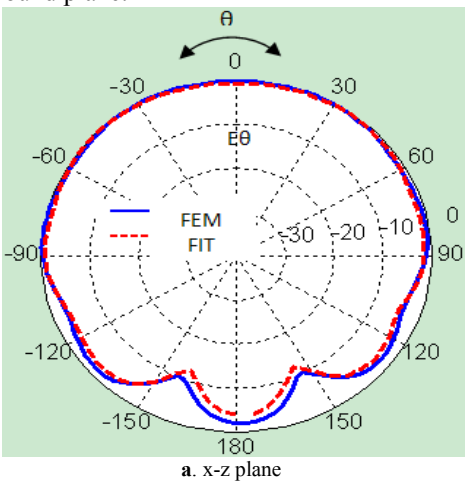

a. x-z plane

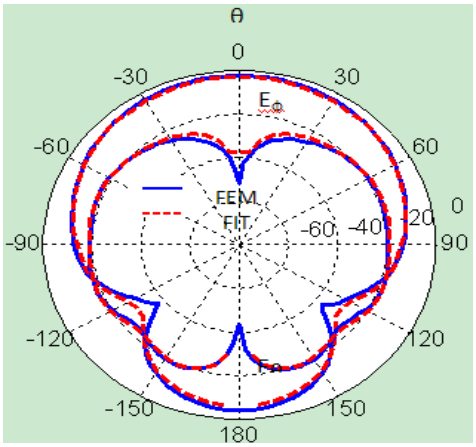

b. y-z plane

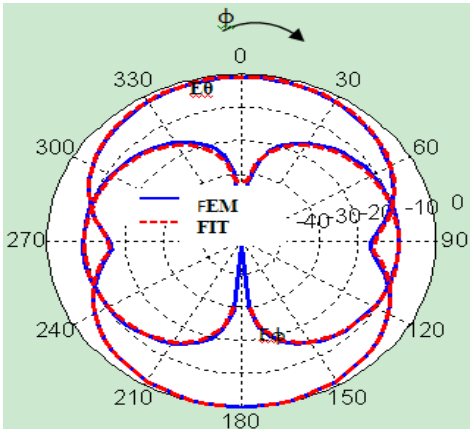

c. x-y plane

Figure 7. The radiation patterns in different planes at f= 1.77GHz.

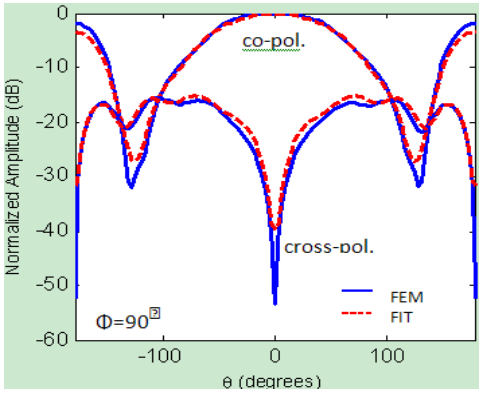

(a)

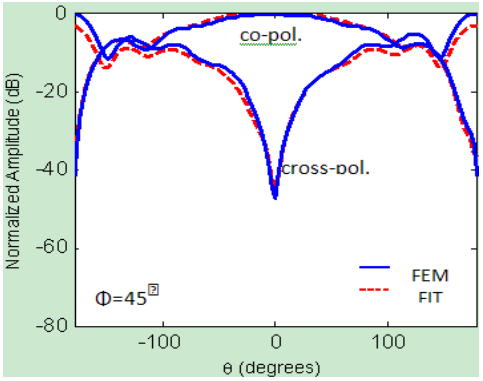

(b)

Figure 8. Radiation patterns of copolarized and cross-polarized field components at f=1.77 GHz.

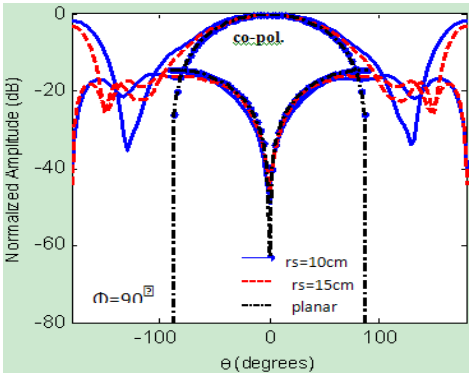

(a)

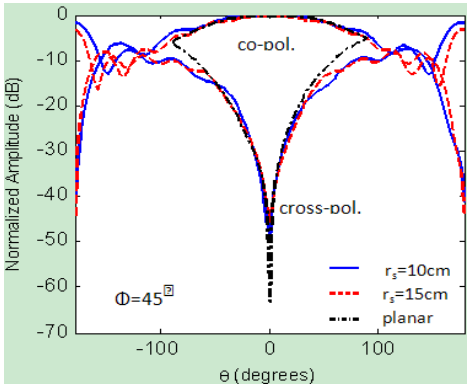

(b)

Figure 9. Radiation patterns of co polarized and cross-polarized field components for different sphere radii, r_s, at f=1.77GHz.

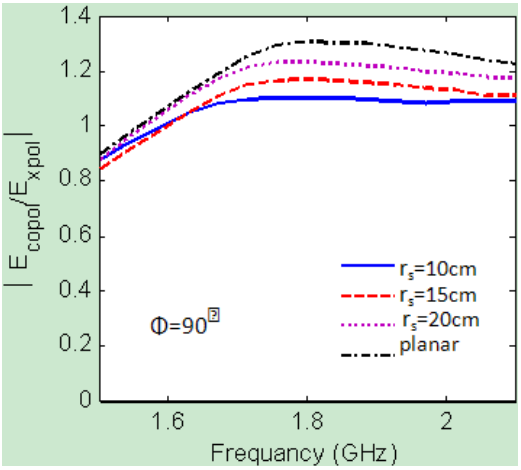

Figure 10. Cross-polarization level as a function of frequency.

A hemispherical DRA embedded in spherical ground plane structure loaded with protecting dielectric superstrate is shown in Figure11. The superstrate layer directly loaded the hemispherical DRA. It has a relative permittivity εrs, a thickness hc = 3.5 cm and rc=4 cm. Figure12 and Figure13 show the variations of reflection coefficient and input impedance with frequency for different superstrate materials εrs. Four cases εrs =1, εrs =2.2, εrs =3.5, and εrs =5.7 are studied. From the results it is seen that both the resonance frequency and the impedance bandwidth are decreased with increasing the relative dielectric constant of superstrate material εrs. The values of the input impedance are changed dramatically with increasing εrs. Figure14 shows the resonance frequency versus the relative dielectric constant of superstrate materials εrs. Figure15 shows the effect of changing the radiation patterns in different planes for different superstrate materials. The operating frequency used for calculating the radiation patterns is f=1. 756GHz. It is observed that the radiation patterns are almost exactly the same for different values of εrs for Eθ component (Figure15a). Little variations in Eφ components in different planes with changing εrs (Eφ very small in x-z plane) are noticed. The changing of the co-polarized and cross-polarized field components are shown in Figure16. The cross-polarization component is increased with increasing dielectric superstrate material εrs. The cross-polarization level as a function of the resonant frequency at different superstrate materials is shown in Figure17. The values of the cross polarization level are dependent on the relative constant of the superstrate material. Figure18. Show the variations of reflection coefficient with frequency for different values of rc. It is noted that the impedance bandwidth are increased with increasing the value of rc (the thickness of dielectric superstrate) and resonance frequency is decreased. Figure19. Shows the effect of changing the gain as a function of frequency in different structures of the ground, when the hemispherical DRA embedded in spherical ground plane structure loaded with protecting dielectric superstrate improve the gain than mounted on spherical ground sphere but reduce the impedance bandwidth as shown in Figure20.

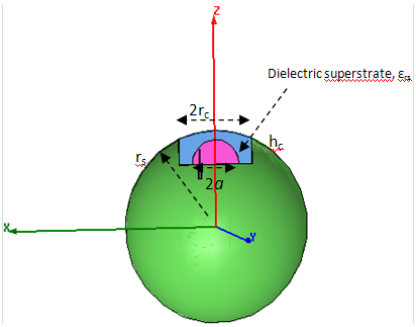

Figure 11. Shows the geometry of hemispherical DRA embedded in spherical ground plane structure.

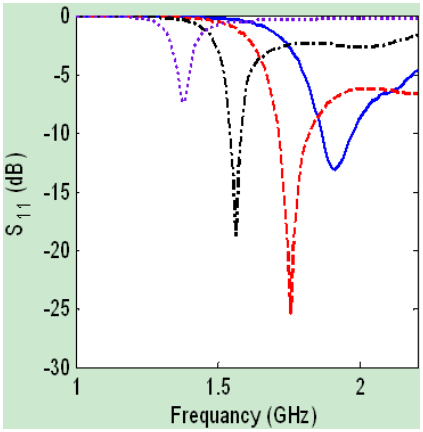

Figure 12. The variation of reflection coefficient versus frequency for different dielectric superstrate, ε_{rs}.

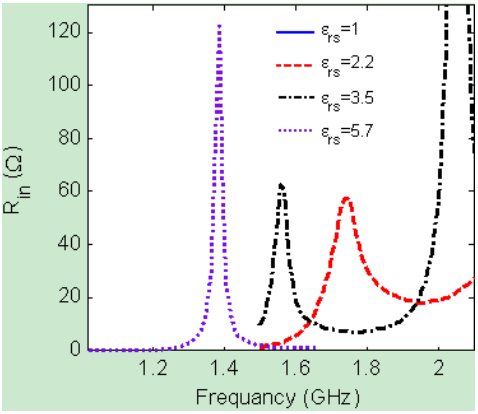

a. input resistance.

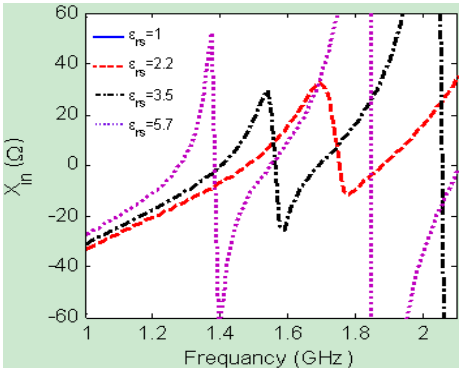

b. input reactance

Figure 13. Input impedance versus frequency for different dielectric superstrate

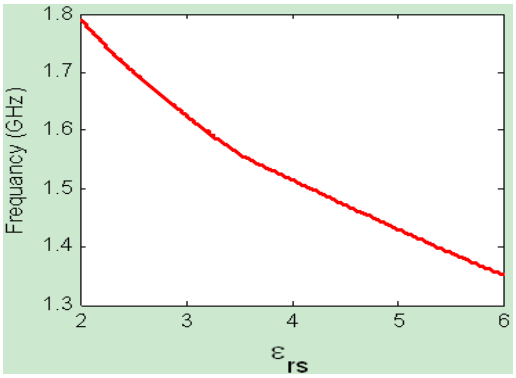

Figure 14. The resonance frequency versus relative dielectric constant of superstrate materials, εrs..

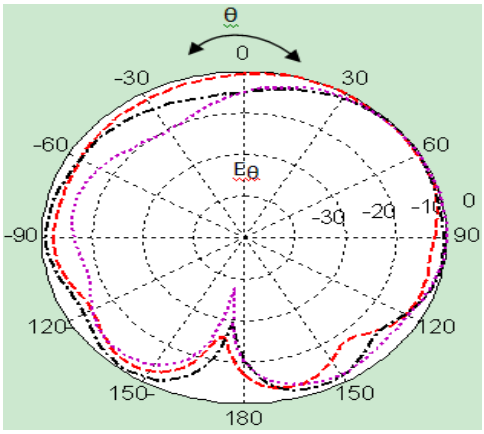

a. x-z plane

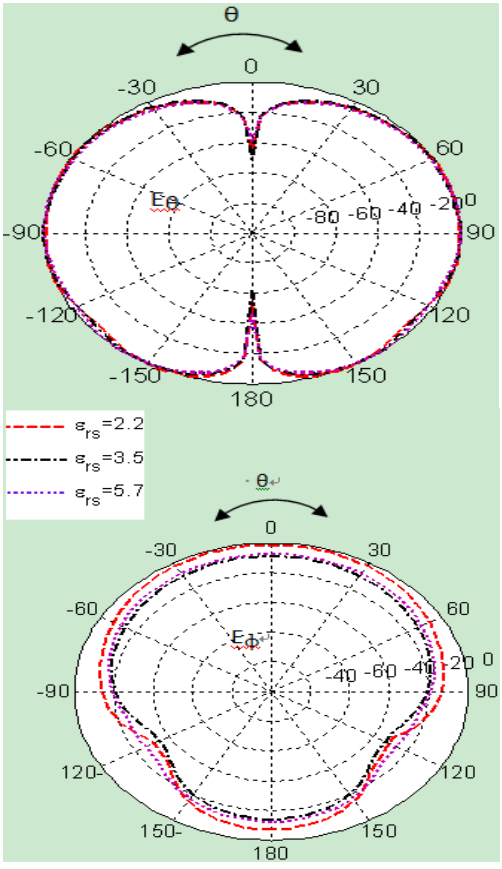

b. y-z

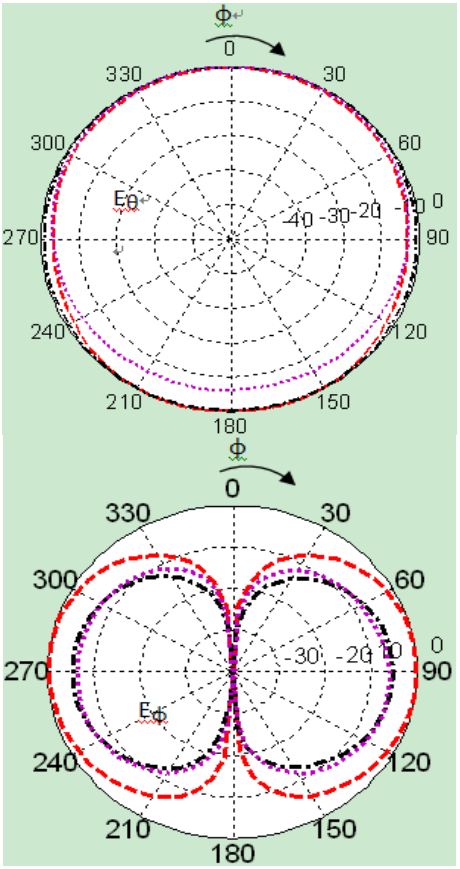

c. x-y plane

Figure 15. The radiation patterns in all planes for different superstrate materials, ε_{rs}, at f=1.756GHz.

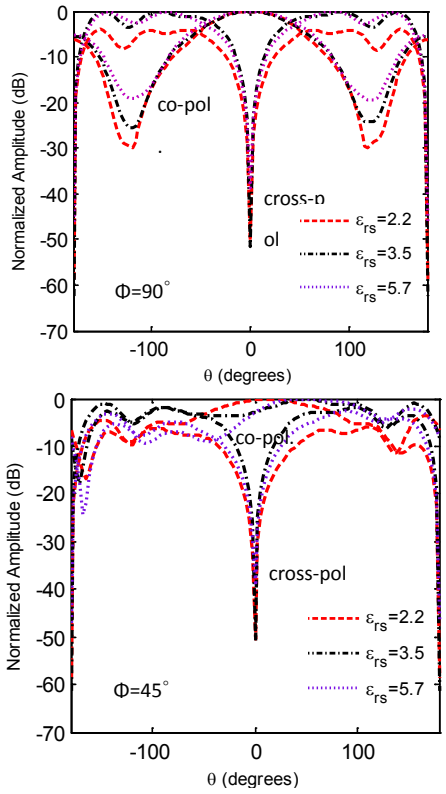

Figure 16. Radiation patterns of copolarized and cross-polarized field components for dielectric superstrate materials, εrs at f=1.756GHz.

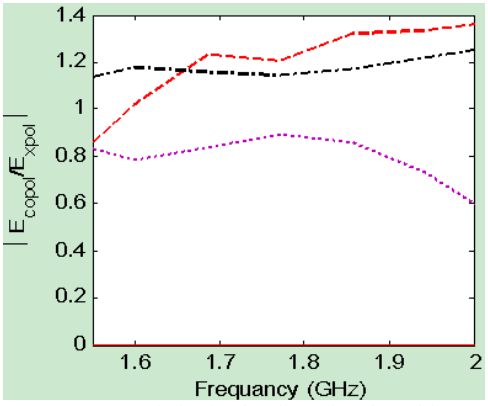

Figure 17. Cross-polarization level as a function of frequency.

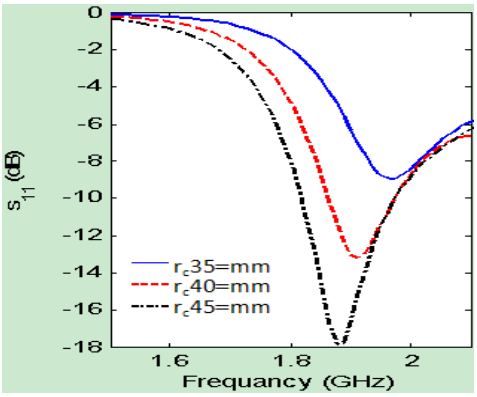

Figure 18. The variation of reflection coefficientVersus of frequency for different r_c.

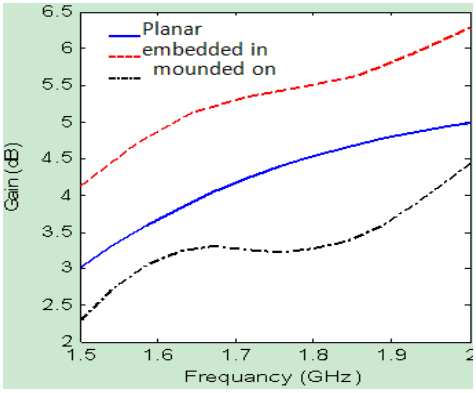

Figure 19. Gain as a function of frequency.

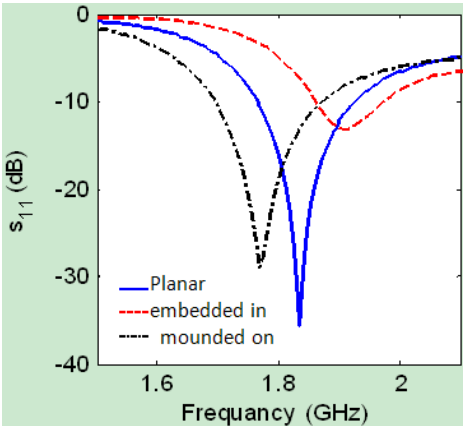

Figure 20. The variation of reflection coefficient versus of frequency.

4. Conclusions

The finite element method and finite integration technique are used to calculate the radiation characteristics of hemispherical DRA mounted on or embedded in spherical ground plane. The hemispherical DRA is loaded with a protecting dielectric superstrate. The effects of changing the radius of the sphere and dielectric superstrate on the reflection coefficient, input impedance, resonant frequency, impedance bandwidth, and radiation patterns in different planes are demonstrated. It is seen that as the radius of the sphere increases the resonance frequency increases, the magnitudes of the input resistance and reactance decrease and the cross-polarization level increases. Also, the cross-polarized field component is increased with increasing the superstrate material. The thickness of dielectric superstrate effect on resonance frequency and the impedance bandwidth then compared between the different grounds structure to show their effect on the gain and impedance bandwidth.

REFERENCES

[1] K.M. Luk, and K.W. Leung, Dielectric Resonator Antenna, Research Studies Press, Hertfordshire, UK, 2003.

[2] G. C. Almpanis, Fumeaux, and R. Vahldieck, "The trapezoidal dielectric resonator antenna," IEEE Transactions on Antennas and Propagation, Vol.56, No.9, pp. 2810-2816, September 2008.

[3] G.P. Junker, A.A. Kishk, and A.W. Glisson, "Input impedance of dielectric resonator antenna excited by a coaxial probe," IEEE Transactions on Antennas and Propagation, Vol.42, No.7, pp. 960-966, July 1994.

[4] A.A. Kishk, Y. Yin, and A.W. Glisson, "Conical dielectric resonator antennas foe wideband applications," IEEE Transactions on Antennas and Propagation, Vol.50, No.4, pp. 469-474, April 2002.

[5] B. Li, and K.W. Leung, "On the differentially fed rectangular dielectric resonator antenna," IEEE Transactions on Antennas and Propagation, Vol.56, No.2, pp. 353-359, February 2008.

[6] T.-H. Chang, and J.-F. Kiang, "Sectorial-beam dielectric resonator antenna for WiMAX with bent ground plane," IEEE Transactions on Antennas and Propagation, Vol.57, No.2, pp. 563-572, February 2009.

[7] A. Petosa, Dielectric Resonator Antenna Handbook, Artech House, Inc., Norwood, USA, 2007.

[8] S. H. Zainud-Deen, H. A. Malhat, and K. H. Awadalla," Dielectric resonator antenna mounted on a circular cylindrical ground plane," Progress In Electromagnetics Research B, PIER B, Vol. 19, pp. 427-444, 2010.

[9] S. H. Zainud-Deen, H. A. Malhat, and K. H. Awadalla," Cylindrical dielectric resonator antenna housed in a shallow cavity in a hollow circular cylindrical ground plane." 26rd Applied Computational Electromagnetics Society (ACES) Conference, Tampere, Finland, April 2010.

[10] J. L. Volakis, A. Chatterjee, L. C. Kempel, Finite Element Method for Electromagnetics : Antennas, Microwave Circuits, and Scattering Applications, IEEE Press, Piscataway, NJ, USA, 1998.

[11] Zhou, X., and G.W. Pan, "Application of physical spline finite element method (PSFEM) to full wave analysis of waveguide," Progress In Electromagnetic Research B, PIER, vol 60, 19-41, 2006.

[12] C. MATTIUSSI, A reference discretization strategy for the numerical solution of physical field problems, Advances In Imaging and Electron Physics, vol. 121, pp. 144-211.

[13] A. C. Polycarpou, Introduction to finite element method in electromagnetics, Morgan & Claypool Publishers' series, USA, 2006.

[14] Z. Chen, and M. Ney, "The method of weighted residuals: a general approach to deriving time and frequency domain numerical methods" IEEE Antennas and Propag. Magazine, vol. 51, no. 1, pp. 51-70, February 2009.

[15] D. Jiao, M. Lu, E. Michielssen, and J. Jin, "A fast time-domain finite element–boundary integral method for electromagnetic analysis," IEEE Trans. Antennas and Propag., vol. 49, no. 10, pp. 1453- 1461, October 2001.

[16] A. Mitchell, D. M. Kokotoff, and M. W. Austin, "Improvement to the PML boundary condition in the FEM using mesh compression" IEEE Trans. Microw. Theory Tech., vol. 50, no. 5, pp. 1297- 1302, May 2002.

[17] T. Weiland, "A discretization method for the solution of Maxwell's equations for six-component fields," Electromagnetics and Communications AEÜ, Vol. 31, No. 3, pp. 116-120, March 1977.

[18] I. Munteanu1 and T. Weiland, RF & microwave simulation with the finite integration technique – from component to system design, Scientific Computing in Electrical Engineering Mathematics in Industry, Volume 11, Part III, pp. 247-260, 2007.

[19] Galina Benderskaya, Numerical methods for transient field-circuit coupled simulations based on the finite integration technique and a mixed circuit formulation, Ph. D. Thesis, Technischen Universit¨at Darmstadt, Darmstadt 2007.

[20] U. van Rienen, "Frequency domain analysis of waveguides and resonators with FIT on non-orthogonal triangular grids," Progress In Electromagnetics Research (PIER 32),pp. 357–381, 2001.